Journal of Biomedical Optics

BiomedicalOptics.SPIEDigitalLibrary.org

Monitoring early phases of orthodontic treatment by means of Raman spectroscopies

Fabrizia d'Apuzzo
Letizia Perillo
Ines Delfino
Marianna Portaccio
Maria Lepore
Carlo Camerlingo

SPIE.

Fabrizia d'Apuzzo, Letizia Perillo, Ines Delfino, Marianna Portaccio, Maria Lepore, Carlo Camerlingo, "Monitoring early phases of orthodontic treatment by means of Raman spectroscopies," *J. Biomed. Opt.* **22**(11), 115001 (2017), doi: 10.1117/1.JBO.22.11.115001.

Monitoring early phases of orthodontic treatment by means of Raman spectroscopies

Fabrizia d'Apuzzo,[a] Letizia Perillo,[a] Ines Delfino,[b] Marianna Portaccio,[c] Maria Lepore,[c,*] and Carlo Camerlingo[d]
[a]Università degli Studi della Campania "Luigi Vanvitelli," Dipartimento Multidisciplinare di Specialità Medico-Chirurgiche e Odontoiatriche, Napoli, Italy
[b]Università della Tuscia, Dipartimento di Scienze Ecologiche e Biologiche, Viterbo, Italy
[c]Università degli Studi della Campania "Luigi Vanvitelli," Dipartimento di Medicina Sperimentale, Napoli, Italy
[d]CNR-SPIN, Istituto Superconduttori, Materiali Innovativi e Dispositivi, Pozzuoli, Napoli, Italy

Abstract. Gingival crevicular fluid (GCF) is a site-specific exudate in the gingival sulcus. GCF composition changes in response to diseases or mechanical stimuli, such as those occurring during orthodontic treatments. Raman microspectroscopy (μ-RS) and surface-enhanced Raman spectroscopy (SERS) were adopted for a GCF analysis during different initial phases of orthodontic force application. GCF samples were pooled from informed patients using paper cones. SERS spectra were obtained from GCF extracted from these cones, whereas μ-RS spectra were directly acquired on paper cones without any manipulation. The spectral characteristics of the main functional groups and the changes in cytochrome, amide III, and amide I contributions were highlighted in the different phases of orthodontic treatment with both SERS and μ-RS analysis. μ-RS directly performed on the paper cones together with proper statistical methods can offer an effective approach for the development of a tool for monitoring the processes occurring during orthodontic treatments, which may help the clinician in the choice of type of treatment individually for each patient and accelerate and improve the orthodontic therapy. [DOI: 10.1117/1.JBO.22.11.115001]

Keywords: Raman spectroscopy; surface-enhanced Raman spectroscopy; gingival crevicular fluid; multivariate analysis; orthodontic tooth movement.

Paper 170479RR received Jul. 21, 2017; accepted for publication Oct. 12, 2017; published online Nov. 6, 2017.

1 Introduction

Orthodontic movements induce tooth repositioning by a gradual remodeling of alveolar bone and periodontal ligament (PDL). This process involves the activation of many complex cellular and molecular mechanisms mediated by the release of chemical substance cascades.[1] The PDL is a membrane-like connective tissue interposed between the tooth root and the alveolar bone. It has an important role in supporting the tooth in the bone socket and in maintaining homeostasis of the surrounding tissues, such as the alveolar bone and cementum.[2,3] The application of orthodontic forces results in the increase and modification of the gingival crevicular fluid (GCF) in the periodontal space due to an inflammatory process occurring as a response to tissue stress.[4,5] GCF is a site-specific exudate deriving from the epithelium lining of the gingival sulcus. The GCF has a complex composition: in addition to blood electrolytes, many organic molecules occur in its formation, such as albumins, globulins, and lipoproteins.[6–8] Leukocytes, neutrophils, and lymphocytes are also expected to be present in the GCF, especially when an inflammatory status is activated.[9] The site-specific nature of GCF collection is useful in monitoring the factors relating to periodontal diseases and can be used for diagnostic purposes.[10] For example, Sharma and Pradeep[11] found an increasing trend of osteopontin level in the GCF by comparing healthy subjects with patients affected by gingivitis or periodontitis. Ngo et al.[12] reported a comprehensive proteomic analysis identifying different proteins and peptides in the GCF. Biochemical assay analysis of the GCF has also been largely used as a noninvasive diagnostic procedure to evaluate the biologically active substances expressed by cells within the periodontium in response to mechanical stimuli due to orthodontic tooth movements.[13–17] These assays are time-consuming, require complicated procedures, and the use of a large number of different chemical products. In addition, the biomarkers are generally evaluated individually, rarely in a small number, and they are not able to give global information. For these reasons, the predictive clinical relevance of potential biomarkers is still under investigation.[18,19]

Conversely, vibrational spectroscopies can constitute an efficient method to obtain an overall biochemical characterization of the GCF and to detect its changes during orthodontic treatments. In fact, these techniques can be used to analyze biological specimens with high sensitivity to subtle chemical and structural changes.[20–22] In recent decades, Raman microspectroscopy (μ-RS) has been demonstrated to be a very effective tool in many biomedical fields[23–27] especially when applied to the analysis of biofluids, i.e., serum, plasma, blood, tears, urine, saliva, and synovial fluid,[23,24,28,29] being almost insensitive to the presence of water. Biofluids can be used for routine clinical applications since they can be easily collected by a minimally invasive method and can be repeatedly available for monitoring disease progression or therapeutic response.[29] In addition, μ-RS requires simple or no preparation of the samples.

Recently, μ-RS has been used to assay GCF changes during the initial phases of orthodontic tooth movements.[30–32] In

*Address all correspondence to: Maria Lepore, E-mail: maria.lepore@unicampania.it

1083-3668/2017/$25.00 © 2017 SPIE

particular, Jung et al.[31] investigated GCF samples obtained before and during an orthodontic treatment (before and after 2, 7, and 28 days from the beginning). They performed μ-RS measurements on a drop of GCF deposited on a gold-coated substrate using a 100-mW 785-nm diode laser source. They noticed that the intensity ratios of some peaks such as phosphate to amide I and phosphate to carbonate change indicating demineralization effects during the process of alveolar bone remodeling. They also reported significant changes in the amide I band during the orthodontic treatment.

In our previous studies, we used μ-RS for investigating GCF directly on the paper cones generally used for pooling the fluid during an orthodontic treatment with conventional fixed appliances (before and after 2, 7, and 14 days from the beginning of the treatment).[30,32] No manipulation of the samples was required, and a rapid examination of the GCF was obtained using a commercial system equipped with a 17-mW 633-nm helium–neon laser. This low-intensity level ensured that no heat degradation of the samples occurred during measurements. These preliminary results indicate that it is possible to collect significant GCF Raman spectra directly on paper cones and confirmed the modifications of amide I band during the orthodontic treatment. In addition, certain changes in protein content were also noticed.[32]

In order to enhance GCF analysis before and during orthodontic treatments, we used the already adopted μ-RS, and we employed surface-enhanced Raman spectroscopy (SERS) to obtain more detailed GCF spectra. In fact, SERS technique can be extremely useful when samples are characterized by a low signal as in the case of GCF.[33–37] For this kind of measurement, we followed the same procedure of Jung et al.[31] for extracting the fluid from paper cones, and we used substrates prepared with homemade gold nanoparticles (GNPs).[38] Furthermore, we widened our investigation on μ-RS measurements directly performed on impregnated paper cones to a large number of patients.

SERS measurements allowed us to obtain spectra clearly showing the contributions of the main functional groups of GCF components and to observe their changes, which related to the different stages of orthodontic treatments. Furthermore, the results of μ-RS of the GCF on impregnated cones, together with the use of a numerical classification method of the spectra and a multivariate analysis, were shown to offer a proper approach for the development of a tool for routinely monitoring the processes occurring during an orthodontic treatment. Such a tool can assist clinicians in the selection of the type of treatment for each patient and in the improvement of the treatment itself.

2 Materials and Methods

2.1 *Subjects*

GCF samples were pooled from patients aged between 12 and 22 years consecutively recruited at the Orthodontic Program of the Università della Campania "Luigi Vanvitelli," Naples, Italy, from December 2015 to December 2016 (see Table 1). Informed consent was obtained from each minor patient's parents or adult patients after providing them with detailed information about the study. Ethical approval for this study was granted by the Ethics Board of the above-mentioned university.

The inclusion criteria were as follows: nonextraction fixed orthodontic treatment required, permanent dentition with similar incisor irregularity index in the mandibular dental arch ($\geq$2), a good general healthy periodontium with no radiographic evidence of bone loss, no gingival inflammation and probing depth of 3 mm in the whole dentition, and a full-mouth plaque score and a full-mouth bleeding score $\leq$ 20%.[39] Exclusion criteria included previous orthodontic treatment with fixed appliances, history of systemic diseases, congenital deformities, mandibular tooth agenesis, previous periodontal disease, and the use of antibiotic or antiinflammatory drugs in the month preceding the beginning of the study. Moreover, drug consumers and smokers were also removed from the study.

For this study, we utilized a 50 gr Sentalloy® (GAC International, Bohemia, New York) coil spring *in vivo*. Orthodontic brackets with power pin (MBT; 3M Unitek; Monrovia; Cali, Colorado) were applied on the buccal surface of the upper and/or lower first premolars and bands were placed on upper and/or lower first premolar only on the right side. Bracket bonding, arch-wire insertion, and ligation were performed by the same operator.

2.2 *Collection and Preparation of GCF Samples*

The GCF samples were collected from each patient before bracket bonding (T0), and after 2 (T1), 7 (T2), and 14 (T3) days of treatment at the buccal side of the incisors. The T0 samples represented the controls. Before GCF collection, the sample

Table 1 Year of birth and gender of patients considered in the present study.

Patient code	Year of birth	Sex
A	2001	M
B	2003	M
C	1993	F
D	2006	M
E	2004	M
F	2002	F
G	2002	F
H	2004	M
I	2002	M
J	2005	M
K	2005	M
L	2000	M
M	1993	M
N	1999	M
O	1999	F
P	1998	M
Q	1998	M
R	2004	F

contamination by blood, saliva, and plaque was minimized by using suction and self-retaining retractor, and the target teeth were carefully cleaned, gently dried with air stream for 5 s, and isolated with cotton rolls. Standardized sterile absorbent paper cones were inserted 1 mm into the gingival crevice and left *in situ* for 30 s, without blood, saliva, and plaque contamination. Two cones were consecutively used (1-min interval) in order to maximize GCF volume per site. Paper cones were transferred to sterile plastic vials and stored at −80°C. These paper cones were used without any other treatment for μ-RS measurements. Immediately before SERS measurements, 10 μL of distilled water was added and the tubes were vortexed for 30 s and centrifuged (10 min, 800 g).

2.3 *Nanoparticle Preparation and Characterization*

GNP preparations were obtained by conventional citrate reduction method.[38,40] The amount of sodium citrate was defined in order to obtain GNPs with an expected diameter of about 30 nm since preliminary measurements showed that this was a good choice for SERS applications.[38] Particle size and stability of the resulting preparations were investigated by means of absorption spectroscopy, transmission electron microscope (TEM), and dynamic light scattering (DLS). In particular, absorption spectroscopy was used to obtain information on the plasmon resonance peak and to study the stability of the preparations. TEM and DLS were used to evaluate the size of the GNPs. A mean GNP diameter of 30 nm was estimated from the observed plasmon resonance band maximum position using the tabular data reported in Ref. 41. Moreover, the absorption spectra remained unchanged for a long time suggesting a stability of the preparation of more than 6 months. TEM results were in agreement with those from DLS and provided a mean diameter for the GNPs of 27 ± 7 nm. For further details, see Ref. 38.

2.4 *Raman Microspectroscopy and SERS*

2.4.1 *Spectra acquisition*

GCF samples were excited by the light of a He—Ne laser operating at a wavelength $\lambda = 633$ nm, with a maximum nominal power of 17 mW. The signal was collected by a Jobin-Yvon TriAx 180 monochromator, equipped with a liquid N_2-cooled CCD and a grating of 1800 grooves/mm, allowing a spectral resolution of 4 cm^{-1}. For μ-RS, the laser light was focused on the sample surface by means of a 100× optical objective (n.a. = 0.90) on an excitation spot area of about 5 μm of size. The spectra were obtained using accumulation times ranging from 60 to 300 s. SERS spectra were collected using the same apparatus equipped with a 50× (n.a. 0.75) objective (excitation spot size of about 10 μm of size) and by adopting an accumulation time of 300 s. For this kind of measurement, a drop of the GNP solution was placed on a microscope glass and left to dry for some hours. A small amount (5 μL) of the GCF sample was then deposited on the microscope glass decorated with dried GNP preparation and immediately after SERS measurements were performed. The Raman spectrum of the dried GNP solution was recorded for the 200 to 3200 cm^{-1} spectral range and, as expected, an unfeatured signal with a broad peak located at around 2800 cm^{-1} was observed. In general, no features due to the GNPs were present in the 200 to 1800 cm^{-1} range, which is the region of interest of the present study.[38]

For μ-RS measurements, the paper cones with GCF were directly examined. μ-RS was also performed on a pristine paper cone (without GCF) under experimental conditions similar to those used for sampling GCF to distinguish the signal from the substrate contribution.

2.4.2 *Background subtraction*

The Raman spectra collected from GCF samples showed a smeared background signal that was even able to reach 80% of the whole average intensity. In order to enhance the signal readability and to attenuate the background and noise components, an automatic numerical treatment based on a wavelet algorithm was used.[25,42] After the wavelet-based data treatment, the Raman spectra of GCF samples were compared to the paper cone spectrum by linear regression analysis. Then, the Raman spectrum from the paper cone was subtracted from the GCF signal, using the regression coefficient as a scaling factor for signals. In the case of SERS measurements, the data treatment was limited to the removal of the background component of the signal using the wavelet-based procedure described above.

2.4.3 *Spectra deconvolution*

The spectra were analyzed in terms of convoluted peak functions to determine the basic vibrational modes that contribute to the Raman signal using a best-fit peak fitting routine of the GRAMS program, based on the Levenberg–Marquardt nonlinear least-square method.[43] Lorentzian peak shape was used. Peaks constituting the spectrum were manually selected in order to define the starting conditions for the best-fit procedure. The best-fit was then performed to determine the optimized intensity, position, and width of the peaks. The performance of the procedure was evaluated by means of the χ^2 parameter.[44] The band of amide I (located in the 1550- to 1750-cm^{-1} wavenumber region) was analyzed in detail since significant variations were expected due to protein configuration changes.

2.4.4 *Ranking analysis*

In order to determine a selection criterion able to distinguish the differences occurring in GCF due to the orthodontic process, we numerically analyzed the spectra using some statistical tools enclosed in the "Bioinformatics Toolbox" of MATLAB® software package (Version 7.6, MathWorks Inc., Natick, Massachusetts). They are typically employed for processing large data files, as those produced by mass spectrometry measurements, and are here used for the first time to our knowledge for processing Raman spectra. The adopted procedure enabled us to select a reduced set of spectral points or "features" that may be used to distinguish Raman spectra acquired from patients at different stages of the orthodontic treatment.

GCF Raman spectra resulting from the wavelet data treatment were considered. First, "rankfeatures(X, group)" subroutine allowed us to rank the Raman spectra (X) using an independent evaluation criterion for binary classification in different prefixed "groups." In the first step of the analysis, two groups were considered: the "T0 group," including the T0 spectra, and the "T1 + T2 group," including the T1 and T2 spectra. Basically, the program selected 10 points of the spectra (wavenumber positions) where the differences between the elements of the two groups are more significant. The group membership was determined by comparing the Euclidean distances between

the different elements of the two groups.[45] After the first discrimination step, the spectra classified in the T1 + T2 group were elaborated again and classified in the two T1 and T2 subgroups. Details of the algorithm used are reported in Appendix A.

2.4.5 *Multivariate analysis (i-PCA)*

Among multivariate analysis methods, those based on the principal component analysis (PCA) proved to be particularly suitable for analyzing the complex spectra resulting when Raman spectroscopy is used in biomedical applications.[46,47] The PCA method performs a mathematical decomposition of the spectral data, which reduces the data dimensions to a smaller number of scores and principal components (PCs) or loadings that effectively carry most of the important information of the spectra.[48] Classification of spectral data can be easily done by choosing different combinations of PCs to build a new coordinate system. When the PCA analysis is performed on selected wavenumber ranges of the Raman spectra, information embedded in those specific ranges can be better outlined. This is the case of interval-PCA (i-PCA)[44,49,50] that was used for analysis in the present case. Here, i-PCA was performed on the wavelet-treated GCF Raman spectra using the narrow spectral regions (called relevant intervals, RI; their number being nRI = 20) outlined in the previously described ranking analysis (see Appendix A).

Once i-PCA was performed, each spectrum was described using the scores of the first three PCs found in the RIs. As usual, the PCs are ordered according to the percentage of the explained variance, from the highest to the lowest value. It was checked that this number of PCs was sufficient to explain at least 90% of the total variance in each relevant interval.

The dataset resulting from the use of the new variables (dataset dimension: three times nRI for each spectrum) was used to build a classification model, considering three distinguished prefixed groups (i.e., T0, T1, and T2). It was built by using the dataset as a training set and the information about the group to which each spectrum truly belongs. The model was then used to classify each spectrum that in turn was used as an unknown sample.

In addition, MATLAB® software package was employed for this analysis by means of home-written scripts using MATLAB® Statistical Toolboxes and i-PCA toolboxes.[44,49] The i-PCA analysis was performed on the complete dataset by analyzing the covariance matrix after subtracting the mean of the variables. The classification was done by using the built-in function "classify" by performing a fit of the multivariate normal densities considering a diagonal covariance matrix estimate (naive Bayes classifiers).

3 Results and Discussion

3.1 *SERS Measurements on GCF Liquid Samples*

A typical SERS spectrum obtained from GCF samples pooled from a patient before starting the previously described orthodontic treatment is reported in Fig. 1 in the range from 400 to 1800 cm^{-1} together with the results of the deconvolution procedure adopted for determining the principal vibrational modes. In this spectrum, it is possible to highlight different contributions due to the various components of GCF. In particular, the feature observed at 465 cm^{-1} can be ascribed to S—S bond stretching.[51] The structures at 621 and 825 cm^{-1} are attributed to phenylalanine and tyrosine contributions, respectively.

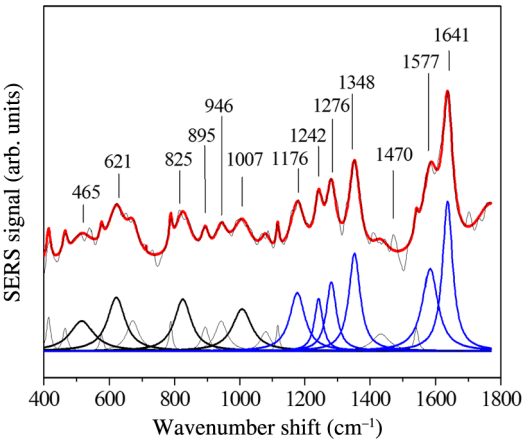

Fig. 1 SERS spectrum of a GCF sample collected before orthodontic treatment (T0). The experimental data are fitted by a convolution of Lorentzian peaks (red line). The positions of the main deconvoluted modes are indicated. The component modes are reported on the bottom of the figure, arbitrarily shifted along the *y*-axis.

The small peaks at 895 and 946 cm^{-1} can be assigned to the nucleic acid backbone and PO_4^{3-}. The peak at 1007 cm^{-1} is due to C—H bending phenylalanine contribution. The mode at 1176 cm^{-1} can be attributed to the nucleic acid base C—N. The peaks at 1242 and 1276 cm^{-1} can be due to different components of amide III (α-helix or β-sheet) and the 1276 cm^{-1} peak may also indicate a contribution from CH_2 deformation mode. The peak observed at 1348 cm^{-1} can be assigned to adenine/guanine of nucleic acids. The small peak at 1470 cm^{-1} is due to CH_2, the one at 1577 cm^{-1} can be related to amide II and cytochrome, and the large structure at 1641 cm^{-1} is typical of protein spectra and is related to amide I. All the structures highlighted are reported in Table 2 along with their assignments according to Refs. 44, 51, 52 and references therein.

SERS spectra of the GCF collected from an 18-year-old patient (*N* patient) are shown in Fig. 2 for T0 (before treatment beginning), T1 (after 2 days), T2 (after 7 days), and T3 (after 2 weeks) stages of the orthodontic treatment. The application of stress on the tooth induces changes in the GCF composition that can be seen in the SERS spectra. We focused our attention on the 1000 to 1700 cm^{-1} wavenumber range and on the five main modes at about 1176, 1276, 1348, 1577, and 1641 cm^{-1} (see Fig. 2, T0 spectrum). As the time elapsed from the beginning of the orthodontic process increases, the intensity of Raman mode at 1276 cm^{-1} decreases. Conversely, the amide I band intensity increases in the T1 stage with respect to T0 (see T1 spectrum in Fig. 2) and decreases in the subsequent T2 and T3 steps. This behavior can be ascribed to changes in protein concentration. A similar effect has been observed by Jung et al.,[31] and it is also expected because it is well known that orthodontic treatment induces inflammatory processes and changes in cytokines, enzyme, and metabolites concentrations.[1,4,5,14–17] These changes are more intense immediately after the application of orthodontic forces and decrease over time. In addition, the center of the amide I band shifts toward a lower wavenumber shift value (from 1641 to 1611 cm^{-1}) reflecting changes in the protein configuration.[30] As far as concerns amide I band shift, Jung et al.[31] noticed a spectral blueshift differently from us.[30,32] Moreover, observing T1, T2, and T3 spectra, a significant increase in the intensity of the modes at 1167, 1390, and 1577 cm^{-1} is found. The mode at

Table 2 Main peaks observed in SERS spectra of GCF samples collected at different stages of the orthodontic treatment and relative assignments according to Refs. 44, 51, and 52.

Mode position (cm^{-1})			
Before	2 to 7 days	14 days	Assignment
465			S—S bond stretching
621			Phenylalanine
825			Tyrosine
895			Nucleic acid backbone
946			PO_4^{3-}-phosphate (hydroxiapatite)
1007			C—H bending phenylalanine
	1167	1167	Cytochrome
1176			Nucleic acid base C—N
1242	1242		Amide III
1276			Amide III/CH_2 deformation
1348	1348		Nucleic acids (adenine/guanine)
		1390	Cytochrome
1470			CH_2
1577	1577	1577	Amide II/cytochrome
		1611	Amide I
1641	1641		

1577 cm^{-1} is also visible in the T0 spectrum as a shoulder of the amide I band. All these modes are compatible with the Raman vibrations of cytochrome complex, a small heme-protein with high oxidation properties.

More detailed information can be obtained from the amide I band deconvolution [Fig. 3(a)]. During the orthodontic treatment, the center of amide I band moves toward shorter

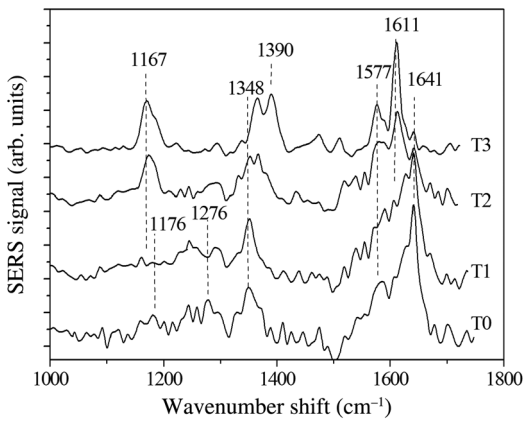

Fig. 2 SERS spectra of GCF samples collected from an 18-year-old patient (N) before (T0), after 2 (T1), after 7 (T2), and 14 days (T3) the beginning of the orthodontic treatment. The spectra are arbitrarily shifted along the *y*-axis.

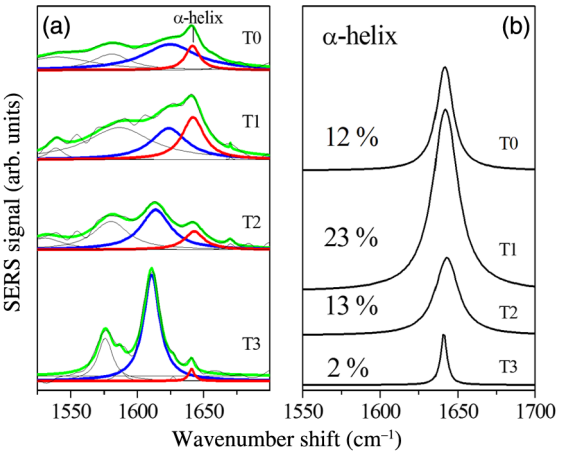

Fig. 3 (a) Amide I region of SERS spectra of GCF samples collected from an 18-year old patient (N) before the beginning of the orthodontic treatment (T0) and 2 (T1), 7 (T2), and 14 (T3) days after. The experimental data (black line) are fitted by a convolution of Lorentzian peaks (green line) and the main components are plotted. The α-helix and the β-sheet components of amide I band are emphasized by the red and blue lines, respectively. (b) The α-helix component at T0, T1, T2, and T3 stages. The spectra are arbitrarily shifted along the *y*-axis. Percentage value of the of the α-helix area normalized to the whole amide I band area is reported for each plot.

wavenumber shifts, especially in T2 and T3 spectra. This is due to the decrease of the α-helix contribution (located around 1640 cm^{-1}) and the increase of the β-sheet contribution (located in the range between 1610 and 1625 cm^{-1}). The percentage of α-helix contribution to the amide I band was estimated by the ratio of areas of the α-helix peak and the whole amide I band, and it is reported for the different stages of treatment in Fig. 3(b). After an initial increase of the α-helix contribution at T1, a decrease at T2 and T3 is observed. The differences in the behavior of the amide I contributions at the different stages observed by Jung et al.[31] could be ascribed to different GCF sampling and days of collection.

3.2 *μ-RS on Paper Cones*

With the aim to develop a simple and minimally invasive method for monitoring the orthodontic treatment, a micro-Raman analysis directly on the impregnated GCF paper cones without any sample manipulation was performed. In Fig. 4, the Raman spectra of the GCF from two patients (E and P) before treatment (T0) are reported. Also in these spectra, it is possible to point out some of the features already observed in the SERS spectrum (Fig. 1). The two main broadbands located at around 1250 to 1275 and 1640 cm^{-1} can be assigned to amide III and amide I, respectively. Moreover, modes due to the nucleic acids can be found at wavenumber shift positions of 1176 and 1348 cm^{-1}. Finally, the 1575- to 1577-cm^{-1} mode is considered as a shoulder of the amide I band.

The μ-RS spectra collected after 2 days (T1) and 7 days (T2) from the beginning of the orthodontic treatment are reported in Fig. 5, along with the corresponding T0 spectra for the same two patients in Fig. 4. In particular, Fig. 5(a) shows spectra from P patient samples and Fig. 5(b) shows those from E patient. In both cases, an increase of the intensity of the Raman modes around 1100 cm^{-1} (due to PO_2^- of nucleic acids[51]) and 1348 cm^{-1} is observed. The intensity of the 1575-cm^{-1}

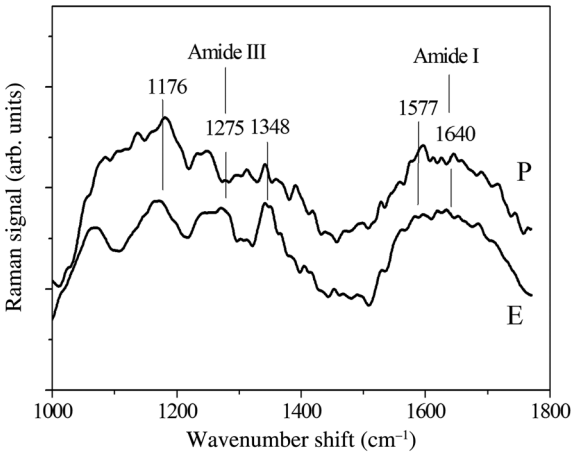

Fig. 4 Representative μ-RS spectra of GCF samples on paper cones collected before the beginning of the orthodontic treatment (T0) from two patients: 12-year old (E) and 16-year old (P). The spectra are arbitrarily shifted along the *y*-axis.

mode also increases, even if more noticeably in samples from P patient [Fig. 5(a)]. This feature confirms an increase of cytochrome content of the GCF during the orthodontic force application also supported by the occurrence of a peak at 1372 cm^{-1} in the T2 spectra from E patient [Fig. 5(b)], close to the cytochrome mode expected at 1390 cm^{-1} (see Table 2). Amide III band (1280 cm^{-1}) dependence on the treatment stage is different for E and P patients, as evident in T1 and T2 spectra. The differences observed in the spectra from these two patients can be ascribed to their different ages, which may induce a difference in the biological response to the orthodontic treatment.[17] Moreover, a weak peak at about 1450 to 1470 cm^{-1} seems to indicate the presence of lipids at stages T1 and T2 for both patients. The main results of the μ-RS on GCF impregnated paper cones are summarized in Table 3.

Additional information can be obtained by analyzing in more detail the 1500- to 1750-cm^{-1} region where the amide I band is located. In agreement with SERS results, in the μ-RS spectra the center of the band also moves toward shorter wavenumber shifts after the beginning of the treatment. In Fig. 6, the results of the deconvolution procedure for the above-mentioned region are

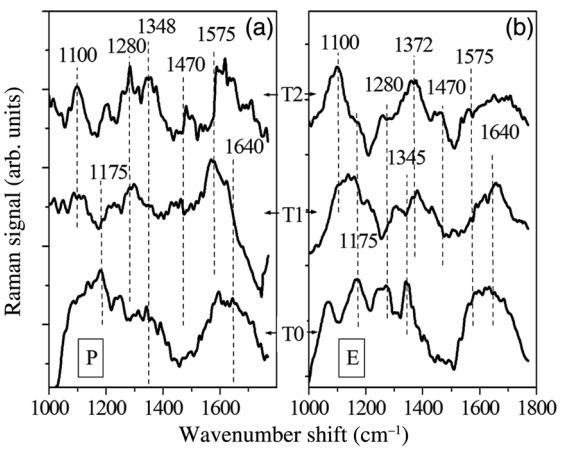

Fig. 5 μ-RS spectra of GCF samples on paper cones collected from the patients (a) P (16-year old) and (b) E (12-year old) before the beginning of the orthodontic treatment (T0) and 2 (T1) and 7 (T2) days after. The spectra are arbitrarily shifted along the *y*-axis.

Table 3 Main peaks observed in μ-RS spectra of GCF samples on paper cones collected at different stages of the orthodontic treatment and relative assignments according to Refs. 44, 51, and 52.

Mode position (cm^{-1})		
Before	2 to 7 days	Assignment
	1100	Nucleic acid base PO_2^-
1176		Nucleic acid base C—N
1276		Amide III
1345		Nucleic acids (adenine/guanine)
1575	1577	Amide II/cytochrome
1640	1625	Amide I

reported for the spectrum of P patient. Also, in this case, Lorentzian peaks were considered and a dependence of their characteristics on the treatment stage can be observed as evident by inspecting the figure, where bold lines indicate the main components of the amide I band. In particular, the red line represents the most relevant contribution (α-helix), which shows a clear shift toward shorter wavenumber shifts. However, the quality of μ-RS spectra is lower than that obtained by SERS and thus a quantitative estimate of the different components is less accurate. Moreover, the deconvolution procedure highlighted an intense peak at about 1540 cm^{-1} appearing at T1 and T2 stages, which can be assigned to carotene.[30,32]

A patient-dependent variability of data is clearly shown, and it has to be considered using proper statistical methods in order to exploit μ-RS directly from GCF impregnated cones for monitoring the orthodontic treatment. For this objective, the

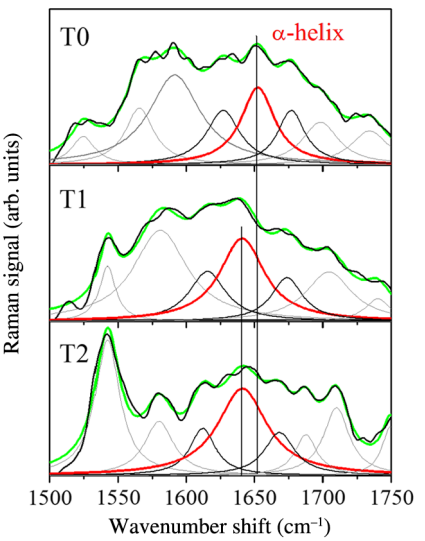

Fig. 6 μ-RS spectra of the amide I region for GCF measured on paper cones at different stages of the orthodontic treatment: T0, T1, and T2. The experimental data (black line) are fitted by a convolution of Lorentzian peaks (green line) and the components are shown. The α-helix component of amide I band is reported by the red line and its center redshifts when the orthodontic treatment is prolonged. The intense peak at about 1540 cm^{-1} appearing at T1 and T2 stages is assigned to carotene.

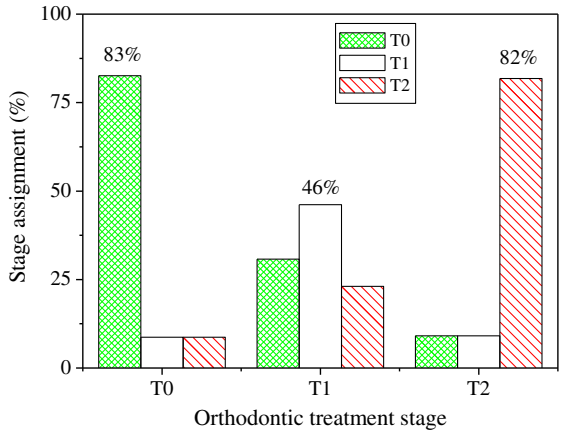

Fig. 7 Percentage of success in the orthodontic treatment stage obtained by comparing the Raman spectra using the ranking analysis. T3 stage was not considered in this analysis due to the limited number of spectra.

proposed approaches for statistical analysis (see Sec. 2.4) were applied to all the Raman spectra of GCF samples before the beginning and at the different stages of the treatment.

The percentages of stage assignment obtained using the ranking analysis is shown in Fig. 7. The rate of success in the determination of the stage is about 83% for T0 and T2 stages, indicating reasonable efficiency of the Raman analysis. A lower percentage of success, about 46%, is found in the T1 spectra. The efficiency in the determination of T1 state is relatively low because several spectra belonging to the T1 class are classified as T0 or T2. This can be attributed to patient-dependent variability. The T3 stage was not considered in this analysis due to the limited number of available spectra. Notably, the features determined using ranking analysis (indicated in Appendix A) are related to the main Raman fingerprints of proteins, DNA, and lipids.[44]

The proposed multivariate analysis (i-PCA, see Sec. 2.4.5) offers a more robust method for taking into account the above-mentioned variability. The results of i-PCA analysis for the single intervals give no useful suggestion about models to group the spectra. The score plots for the single intervals do not suggest any simple grouping depending on the time at which the GCF was collected. However, an overall inspection of these plots suggests that some common spectrum characteristics of a specific group are selected using the first three PCs. In order to exploit these outcomes, a dataset with reduced dimensions was built using the scores of the first three components obtained for the RIs and used for classification. The results of the classification procedure are shown in Fig. 8. Notably, the orthodontic treatment stage is correctly assigned in 98% of Raman spectra with 100% of correct assignment for T0 and T2 spectra and 92% of T1 spectra, some T1 spectra being wrongly classified as T0. These results suggest that the analysis of the GCF using Raman spectroscopy and multivariate analysis can properly recognize the stage of the orthodontic treatment. This may lead the way to define a procedure for an easy, efficient, and repeatable follow-up of the orthodontic treatment.

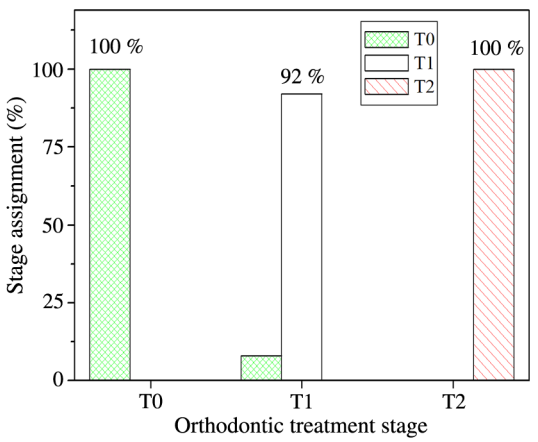

Fig. 8 Percentage of success in the orthodontic treatment stage obtained by comparing the Raman spectra using the i-PCA analysis. Also in this case, T3 stage was not considered due to the limited number of spectra.

4 Conclusions

SERS and μ-RS were adopted to evaluate GCF composition changes due to orthodontic forces in the initial phases of the treatment. The contributions of the main functional groups and the changes related to the different phases of the orthodontic treatment were observed in SERS and μ-RS spectra. In particular, SERS allowed us to obtain spectra with more detailed structures, but changes in cytochrome, amide III, and amide I contributions were evident both in SERS and μ-RS spectra. In addition, the deconvolution of amide I band confirmed the modifications in the secondary structure of protein content. A statistical approach using numerical classification of the spectra and a multivariate analysis indicated that it is possible to assign the GCF to the different stages of treatment.

This study has confirmed that vibrational spectroscopies provide a biochemical analysis of GCF changes during the different stages of orthodontic treatment. In particular, μ-RS analysis directly performed on the paper cones can be an innovative and potential tool for monitoring the complex processes and the patient's response occurring in the early phases of orthodontic treatment. This would be the first step for the development, in the near future, of a Raman spectroscopy-based noninvasive, accurate, and reliable test to monitor the rate of periodontal remodeling during orthodontic tooth movements. It may help the clinician in the choice of the type of treatment individually for each patient. Finally, it may accelerate and improve orthodontic therapy.

Appendix A: Ranking Analysis

As previously mentioned in Sec. 2.4.4, we used the function "rankfeatures" that compares a set of Raman spectra assuming the wavenumber ν as an independent variable, computes a two-way t-test and returns an index of the most significant ν values.

The two-way t-test assigns a single parameter t to each value ν of the spectrum defined as

$$t = \frac{\overline{y_1} - \overline{y_2}}{\sqrt{\frac{S_x^2}{n} + \frac{S_y^2}{m}}},$$

where $\overline{y_1}$ and $\overline{y_2}$ are the intensity mean values of the spectra belonging to group G_0 (containing n elements) and group G_1 (containing m elements), respectively. S_x and S_y are the corresponding standard deviations. The following statement was used in the program:

$$[\text{feat, stat}] = \text{rankfeatures(X, group, 'NWeighting', 50, 'NumberOfIndices', 10)};$$

where "feat" is a vector containing the indexes of features, and "stat" is a vector with the absolute value t of the test statistic. "X" is the set of Raman spectra, "group" is a vector with nominal assignment of spectra to two groups, "NWeighting" = 50 is the weighting factor for local correlation of features (the features that are close to already selected features are less likely to be included in the output list), and "NumberOfIndices" = 10 is the number of features required.

Forty-seven data files were considered in the analysis, each one resulting from the average of six Raman spectra (23 files refer to samples collected before treatment, T0 stage, 13 to samples collected after 2 days of treatment, T1 stage, and 11 to samples collected after 1 week of treatment, T2 stage). Before the analysis, the intensities of Raman signals were normalized with respect to the total spectral area.

First, the ranking analysis was applied to discriminate Raman spectra collected before treatment (T0 group) and those collected after treatment (T1 + T2 group). In Fig. 9, the test statistic dependence on wavenumber shift and the 10 spectral points (features) determined are reported.

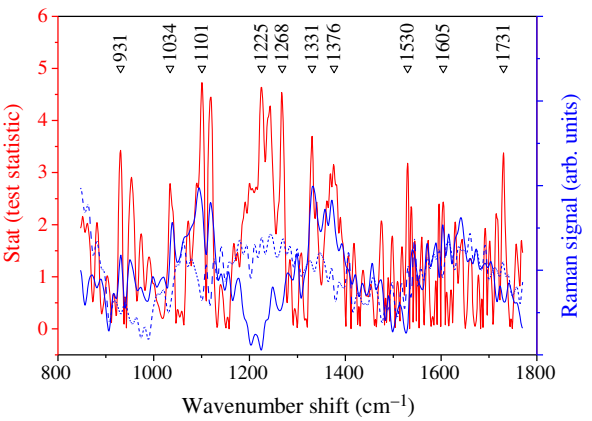

Fig. 9 Statistical results from the comparison of the 47 GCF Raman spectra (red line). Average Raman spectra of T0 group (dotted blue line) and of T1 + T2 group (blue line). The 10 spectral points (features) determined are indicated in the figure.

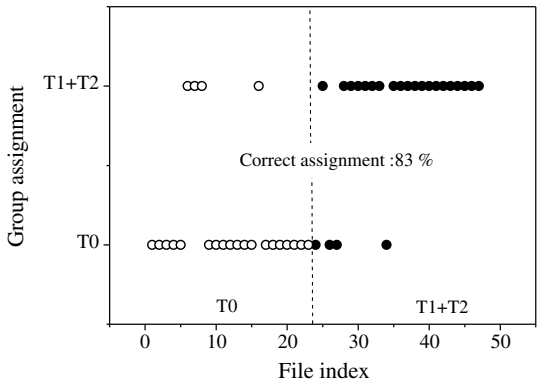

Fig. 10 Group assignment versus file index. The first 23 data points (empty circles) refer to CGF sample collected before treatment (T0 group) and data from 24 to 47 (full circles) to GCF samples after treatment (T1 + T2 group). The success of assignment is 83% for both group T0 and T1 + T2.

In order to quantify the spectral differences, the Euclidean distance between elements of the data file set was calculated by summing the squared differences of spectral values around the "features" points (the five nearest spectral points were considered).[45] The group membership was determined by comparing the Euclidean distances between a selected element and all the other elements of the two considered groups. The group assignment versus file index is reported in Fig. 10. The first 23 data points refer to CGF samples collected before treatment (T0 group) while data from 24 to 47 refer to GCF samples after treatment (T1 + T2 group).

The analysis was applied again on the files assigned to T1 + T2 group in order to discriminate between T1 and T2 spectra. Also in this case, 10 specific features (located at 850, 1008, 1058, 1140, 1219, 1356, 1427, 1524, 1618, and 1767 cm^{-1}) were determined and used.

Disclosures

The authors declare no conflict of interest.

References

1. P. Kapoor et al., "Effect of orthodontic forces on cytokine and receptor levels in gingival crevicular fluid: a systematic review," *Prog. Orthod.* **15**, 65 (2014).
2. G. Anastasi et al., "An immunohistochemical, histological, and electron-microscopic study of the human periodontal ligament during orthodontic treatment," *Int. J. Mol. Med.* **21**(5), 545–554 (2008).
3. F. d'Apuzzo et al., "Micro-Raman spectroscopy investigation on periodontal ligaments: preliminary study on a tissue model," in *Fotonica AEIT Italian Conf. on Photonics Technologies*, pp. 1–3 (2014).
4. S. H. Z. Ariffin et al., "Cellular and molecular changes in orthodontic tooth movement," *Sci. World J.* **11**, 1788–1803 (2011).
5. M. Di Domenico et al., "Cytokines and VEGF induction in orthodontic movement in animal models," *J. Biomed. Biotechnol.* **2012**, 201689 (2012).
6. J. M. Goodson, "Gingival crevice fluid flow," *Periodontology* **31**, 43–54 (2003).
7. M. Rahnama et al., "Gingival crevicular fluid–composition and clinical importance in gingivitis and periodontitis," *Pol. J. Public Health* **124**(2), 96–98 (2014).
8. C. Z. Khurshid et al., "Gingival crevicular fluids (GCF) proteomics: an overview," *Dent. J.* **5**, 12 (2017).
9. B. Shroff, *Biology of Orthodontic Tooth Movement. Current Concepts and Applications in Orthodontic Practice*, Springer International Publishing, Switzerland (2016).
10. K. Nakashima et al., "A longitudinal study of various crevicular fluid components as markers of periodontal disease activity," *J. Clin. Periodontol.* **23**, 832–838 (1996).
11. C. G. Sharma and A. R. Pradeep, "Plasma and crevicular fluid osteopontin levels in periodontal health and disease," *J. Periodontal Res.* **42**, 450–455 (2007).
12. L. H. Ngo et al., "Mass spectrometric analysis of peptides and proteins in human gingival crevicular fluid," *J. Proteome Res.* **9**, 1683–1693 (2010).
13. F. D'Apuzzo et al., "Biomarkers of periodontal tissue remodeling during orthodontic tooth movement in mice and men: overview and clinical relevance," *Sci. World J.* **2013**, 105873 (2013).
14. A. N. Buduneli et al., "Clinical findings and gingival crevicular fluid prostaglandin E2 and interleukin-1-beta levels following initial periodontal treatment and short-term meloxicam administration," *Expert Opin. Pharmacother.* **11**(11), 1805–1812 (2010).
15. G. Barbieri et al., "Biochemical markers of bone metabolism in gingival crevicular fluid during early orthodontic tooth movement," *Angle Orthodontist* **83**(1), 63–69 (2013).

16. M. Grant et al., "Induction of cytokines, MMP9, TIMPs, RANKL and OPG during orthodontic tooth movement," *Eur. J. Orthod.* **35**(5), 644–651 (2013).
17. D. W. J. Rody et al., "Differences in the gingival crevicular fluid composition between adults and adolescents undergoing orthodontic treatment," *Angle Orthodontist* **84**(1), 120–126 (2014).
18. S. Smuthkochorn et al., "Gingival crevicular fluid bone turnover biomarkers: how postmenopausal women respond to orthodontic activation," *Am. J. Orthod. Dentofacial Orthop.* **152**, 33–37 (2017).
19. R. Ahuja et al., "A preliminary investigation of short-term cytokine expression in gingival crevicular fluid secondary to high-level orthodontic forces and the associated root resorption: case series analytical study," *Prog. Orthod.* **18**, 23 (2017).
20. H. J. Butler et al., "Using Raman spectroscopy to characterize biological materials," *Nat. Protoc.* **11**(4), 664–687 (2016).
21. M. J. Baker et al., "Using Fourier transform IR spectroscopy to analyze biological materials," *Nat. Protoc.* **9**(8), 1771–1791 (2014).
22. L. Lovergne et al., "Biofluid infrared spectro-diagnostics: pre-analytical considerations for clinical applications," *Faraday Discuss.* **187**, 521–537 (2016).
23. K. Kong et al., "Raman spectroscopy for medical diagnostics: from in-vitro biofluid assays to in-vivo cancer detection," *Adv. Drug Delivery Rev.* **89**, 121–134 (2015).
24. I. Pence and A. Mahadevan-Jansen, "Clinical instrumentation and applications of Raman spectroscopy," *Chem. Soc. Rev.* **45**(7), 1958–1979 (2016).
25. C. Camerlingo et al., "An investigation on micro-Raman spectra and wavelet data: analysis for pemphigus vulgaris follow-up monitoring," *Sensors* **8**(6), 3656–3664 (2008).
26. C. Camerlingo et al., "Micro-Raman spectroscopy and univariate analysis for monitoring disease follow-up," *Sensors* **11**(9), 8309–8322 (2011).
27. K. A. Esmonde-White et al., "Raman spectroscopy of synovial fluid as a tool for diagnosing osteoarthritis," *J. Biomed. Opt.* **14**(3), 034013 (2009).
28. S. Gonchukov et al., "Raman spectroscopy of saliva as a perspective method for periodontitis diagnostics," *Laser Phys. Lett.* **9**(1), 73–77 (2012).
29. M. J. Baker et al., "Developing and understanding biofluid vibrational spectroscopy: a critical review," *Chem. Soc. Rev.* **45**(7), 1803–1818 (2016).
30. C. Camerlingo et al., "Micro-Raman spectroscopy for monitoring changes in periodontal ligaments and gingival crevicular fluid," *Sensors* **14**(12), 22552–22563 (2014).
31. G. B. Jung et al., "Biochemical characterization of human gingival crevicular fluid during orthodontic tooth movement using Raman spectroscopy," *Biomed. Express* **5**(10), 3510–3520 (2014).
32. C. Camerlingo et al., "Micro-Raman spectroscopy during orthodontic tooth movement: follow-up of gingival status," in *Int. Conf. on BioPhotonics (BioPhotonics '15)* (2015).
33. A. Bonifacio, S. Cervo, and V. Sergo, "Label-free surface-enhanced Raman spectroscopy of biofluids: fundamental aspects and diagnostic applications," *Anal. Bioanal. Chem.* **407**(27), 8265–8277 (2015).
34. S. Schlücker, "Surface-enhanced Raman spectroscopy: concepts and chemical applications," *Angew. Chem. Int. Ed.* **53**(19), 4756–4795 (2014).
35. M. K. Khaing Oo et al., "Gold nanoparticle-enhanced and size-dependent generation of reactive oxygen species from proto porphyrin IX," *ACS Nano* **6**(3), 1939–1947 (2012).
36. Q. Li et al., "Label-free and non-invasive monitoring of porcine trophoblast derived cells: differentiation in serum and serum-free media," *J. Biophotonics* **8**(8), 638–645 (2015).
37. A. Subaihi et al., "Rapid, accurate, and quantitative detection of propranolol in multiple human biofluids via surface-enhanced Raman scattering," *Anal. Chem.* **88**(22), 10884–10892 (2016).
38. C. Camerlingo et al., "Fructose and pectin detection in fruit-based food products by surface-enhanced Raman spectroscopy," *Sensors* **17**(4), 839 (2017).
39. G. Perinetti et al., "Gingival crevicular fluid alkaline phosphate activity during the retention phase of maxillary expansion in prepubertal subjects: a split-mouth longitudinal study," *Am. J. Orthod. Dentofacial Orthop.* **148**, 90–96 (2015).
40. G. Frens, "Particle size and sol stability in metal colloids," *Kolloid-Zeitschrift und Zeitschrift für Polymere* **250**(7), 736–741 (1972).
41. W. Haiss et al., "Determination of size and concentration of gold nanoparticles from UV-vis spectra," *Anal. Chem.* **79**, 4215–4221 (2007).
42. C. Camerlingo et al., "Wavelet data processing of micro-Raman spectra of biological samples," *Meas. Sci. Technol.* **17**(2), 298–303 (2006).
43. D. Marquardt, "An algorithm for least-squares estimation of nonlinear parameters," *J. Soc. Ind. Appl. Math.* **11**(2), 431–441 (1963).
44. I. Delfino et al., "Visible micro-Raman spectroscopy of single human mammary epithelial cells exposed to x-ray radiation," *J. Biomed. Opt.* **20**(3), 035003 (2015).
45. S. Theodoridis and K. Koutroumbas, *Pattern Recognition*, 4th ed., Academic Press, Elsevier Inc., Burlington, Massachusetts (2009).
46. X. Li et al., "Raman spectroscopy combined with principal component analysis and k nearest neighbour analysis for non-invasive detection of colon cancer," *Laser Phys.* **26**, 035702 (2016).
47. J. F. Villa-Manríquez et al., "Raman spectroscopy and PCA-SVM as a non-invasive diagnostic tool to identify and classify qualitatively glycated hemoglobin levels in vivo," *J. Biophotonics* **10**, 1074–1079 (2017).
48. B. G. M. Vandeginste et al., *Handbook of Chemometrics and Qualimetrics*, Elsevier Science, The Netherlands (1998).
49. K. E. Esbensen, *Multivariate Data Analysis-in Practice: An Introduction to Multivariate Data Analysis and Experimental Design*, 4th ed., CAMO–ASA, Oslo, Norway (2000).
50. I. Delfino et al., "Univariate and multivariate analysis of Raman spectra for quantitative determination of sugars in beverage industry," in *Lecture Notes in Electrical Engineering*, Vol. **162**, pp. 375–379, Springer, Heidelberg, Germany (2014).
51. C. David, S. Foley, and M. Enescu, "Protein S─S bridge reduction: a Raman and computational study of lysozyme interaction with TCEP," *Phys. Chem. Chem. Phys.* **11**(14), 2532–2542 (2009).
52. A. J. Hobro et al., "Raman spectroscopy as a tool for label-free lymphocyte cell line discrimination," *Analyst* **141**(12), 3756–3764 (2016).

Fabrizia d'Apuzzo is a PhD student in biochemistry and biotechnology at the Università della Campania "Luigi Vanvitelli." She graduated in dental medicine in 2012 at the same university and received her postgraduate diploma in orthodontics in 2017. She has coauthored over 20 articles and has written three book chapters. Her research interests include biology of tooth movement, vibrational spectroscopies, early treatment, dentofacial orthopaedics, biomechanics, and cleft lip and palate. She is a member of the EOS, WFO, AAO, SIDO, and CH Tweed Foundation.

Letizia Perillo graduated in medicine and surgery and specialized in orthodontics. She did a fellowship at University of Michigan and a PhD at University of Florence. She is a full professor, director of Postgraduate Orthodontic Program, head of Orthodontic Division at University of Campania Luigi Vanvitelli, Naples. She is a member of WFO, AAO, EHASO, EOS, SIDO. She will be SIDO president in 2021. She is author and coauthor of over 300 publications and eight textbooks.

Ines Delfino is an associate professor of physics at the University of Tuscia, Viterbo, Italy. She received her MS degree in physics in 1996 and her PhD in materials engineering in 2001 from the University of Napoli "Federico II." She has coauthored more than 60 journal papers and international volumes. Her current research interests include optical spectroscopies, biophotonics, nanohybrid systems, and multivariate analysis.

Marianna Portaccio is an associate professor of physics at the University of Campania Luigi Vanvitelli, Napoli. She received her MS degree in physics in 1992 from the University of Bari and her PhD in biochemistry and biophysics in 1999 from the University of Padova. She has coauthored more than 70 journal papers and international volumes. Her current research topics are enzyme immobilization, vibrational spectroscopies, and biosensors.

Maria Lepore is an associate professor of physics at the University of Campania Luigi Vanvitelli, Napoli. She received her MS degree in physics in 1982 and her PhD in physics in 1986 from the University of Bari. She has coauthored more than 100 journal papers

and international volumes. Her current research interests are optical spectroscopies, biosensors, and biophotonics for clinical and environmental applications.

Carlo Camerlingo is currently a senior researcher of the National Research Council of Italy (CNR). His research activity regards micro-Raman spectroscopy analysis of biomaterials and innovative technological materials for electronics and sensor applications, as graphene-based structures and iron chalcogenides. This activity includes SERS investigation and the development of methods and processes for micro- and nano-structural engineering. He is an author and coauthor of more than 90 international journal papers.